

A New Cross-Space Total Variation Regularization Model for Color Image Restoration with Quaternion Blur Operator

Zhigang Jia, Yuelian Xiang, Meixiang Zhao, Tingting Wu, Michael K. Ng

Abstract—The cross-channel deblurring problem in color image processing is difficult to solve due to the complex coupling and structural blurring of color pixels. Until now, there are few efficient algorithms that can reduce color infection in deblurring process. To solve this challenging problem, we present a novel cross-space total variation (CSTV) regularization model for color image deblurring by introducing a quaternion blur operator and a cross-color space regularization functional. The existence and uniqueness of the solution is proved and a new L-curve method is proposed to find a sweet balance of regularization functionals on different color spaces. The Euler-Lagrange equation is derived to show that CSTV has taken into account the coupling of all color channels and the local smoothing within each color channel. A quaternion operator splitting method is firstly proposed to enhance the ability of color infection reduction of the CSTV regularization model. This strategy also applies to the well-known color deblurring models. Numerical experiments on color image databases illustrate the efficiency and manoeuvrability of the new model and algorithms. The color images restored by them successfully maintain the color and spatial information and are of higher quality in terms of PSNR, SSIM, MSE and CIEde2000 than the restorations of the-state-of-the-art methods.

Index Terms—Color image restoration; Cross-channel deblurring; Cross-space total variation; Quaternion operator splitting; Saturation value total variation.

I. INTRODUCTION

Blurring process of color image is typically applied to all color channels and is also cross-channel. The observed color pixels may have been affected by neighboring pixels, and there possibly are mutual contamination between their color channels. The classic and latest color image restoration models have made outstanding contributions in this regard. Their innovation focuses on the improvement of regularization terms, while the fidelity items basically follow the classic total variation (TV) model. A long-overlooked, but important, fact is that fidelity items containing blur operators require more accurate characterization and robust algorithms. In this paper, we present a learning regularization term and a new characterization of fidelity item for color image restoration,

School of Mathematics and Statistics & RIIS, Jiangsu Normal University, Xuzhou 221116, P.R. China. E-mail: zhgjia@jsnu.edu.cn

School of Mathematics and Statistics, Jiangsu Normal University, Xuzhou 221116, P.R. China. E-mail: yuelianx@126.com

School of Mathematics and Statistics, Jiangsu Normal University, Xuzhou 221116, P.R. China. E-mail: zhaomeixiang2008@126.com

School of Science, Nanjing University of Posts and Telecommunications, Nanjing 210003, P.R. China. E-mail: wutt@njupt.edu.cn

Corresponding author. Department of Mathematics, Hong Kong Baptist University, Hong Kong. E-mail: michael-ng@hkbu.edu.hk

and also develop a new efficient and fast algorithm to enhance the performance of deblurring.

A color image contains multiple color channels, each of which can be thought of as a binary function. A general color image degradation model is

$$\mathbf{z}(x, y) = \mathbf{K} * \mathbf{u}(x, y) + \mathbf{n}(x, y), \quad (1)$$

where $\mathbf{z}(x, y)$, \mathbf{K} , $\mathbf{u}(x, y)$, $\mathbf{n}(x, y)$ denote degraded color image, blur operator, original color image and additive noise, respectively. Here, $*$ denotes the convolution operator and $\mathbf{K} * \mathbf{u}(x, y)$ characterizes the blurring process. One main task of color image processing is to reconstruct the original color image $\mathbf{u}(x, y)$ from the observed color image $\mathbf{z}(x, y)$. Since the noise $\mathbf{n}(x, y)$ is unknown, one has to inversely solve (1) with minimizing the noise indicator. This unfortunately leads to an ill-posed inverse problem. The way of transforming it into a well-posed problem is to introduce a regularization term into the initial problem. However, the development of color image regularization is blocked for a long time by the difficulty of characterizing complexly coupling and structured blur of color pixels and the hardness to eliminate color infection.

A groundbreaking color image regularization is the (global) channel coupling color TV regularization [1], followed by a local version [2]. These two regularization functionals are based on the RGB color space and couple red, green and blue channels by different norms of TVs on three channels and they can be seen as different norms of vectorial TV of color image. A general framework, called collaborative TV [6], incorporates various norms along different dimensions to provide a comprehensive approach to regularization and the considered norms includes nuclear, Frobenius, and spectral norms. Recently, Duan et al. [5] proposed a new Beltrami regularization model for color image denoising and an efficient and robust operator splitting method, with regarding color images as manifolds embedded in a five dimensional spatial-chromatic space. And a new color elastica model is developed in [17], [18] by using the Polyakov action and a Laplace–Beltrami operator on color channels. These beautiful regularization functionals greatly enrich color image models based on vector representation in one color space.

To find more efficient manners of coupling, various studies explore color space transformation methods to generate regularization functionals on new color space. The chrominance, luminance, or R/B component was formed through a weighted linear combination of the R, G, and B channels of the color image in [3]. This process is also represented as $\sum_k TV(u_k \circ \psi)$

in [6], where ψ is an orthonormal transform to describe the color space transformation. Besides, the human eye is highly sensitive to changes in the opponent color channel. In [25], the opponent transform is employed to transform the RGB color space into the opponent space and the decomposition of the coupling of color channels is allowed. Jia, Ng and Wang [21] recently introduce a saturation-value TV (SVTV) model (given later in (4)) based on quaternion representation of color images. The SVTV regularization functional successfully reflects the physical principle of the human visual system and considers the coupling of red, green, and blue channels. So the SVTV model reconstructs color images of high quality and with slight color infection. The SVTV regularization has been combined with other methods to handle other image processing tasks and the corresponding modified models achieve at a high level on numerical performance; see [13], [31]–[33] for instance.

Above models consider color image restoration in a single color space and their regularizations have been well known for their prior on color edges. Can their advantages be combined into one model? A natural way is to define a learnable regularization term that can characterize the color structures in different color spaces. (See the general model (8).) It is expected to perform better than those with single color space regularization. Color image restoration models with cross color space regularization terms breaks out the limitations in terms of preserving color and texture information. This is shown in Section III-A and also in Section V.

As is well known, the SVTV regularization model is a quaternion-based description [21]. In the actual alternating iteration process, color images are not directly represented and computed by quaternions but by their real counterparts. This conversion of quaternion operations into real operations makes the calculation easier. However, this could cause color infection in the deblurring process (see numerical experiments in Section V). In order not to weaken the advantages of the quaternion model, we need to solve the quaternion model using the quaternion algorithm. In this paper, we further embed quaternion operations in color image cross-channel restoration based on the quaternion operator splitting approach that considers color pixels as quaternions rather than a vectorised representation of individual color channels. Additionally, we directly solve the quaternion linear systems throughout the iterative process using the quaternion Krylov subspace method. This decision will contribute to color fidelity. One effective existing quaternion Krylov subspace method is the quaternion generalized minimal residual method (QGMRES) [22], which can provide more accurate numerical solutions. For details, please refer to [22]. Therefore, the quaternion linear systems in the deblurring process will be solved by the QGMRES method in this paper.

The contribution is in three aspects:

- We present a versatile framework for balanced regularization in multi-color space blending, enhancing color image restoration. This framework contains diverse regularization terms across different color spaces, maintaining color channel relationships and addressing limitations of single-space models. We detail the cross-channel SVTV-CTV

balanced regularization model with RGB and HSV color space regularization and provide theoretical proof of its solution's existence and uniqueness.

- A new algorithm is proposed for the cross-channel SVTV-CTV balance regularization model based on the framework of the alternating minimization method, based on quaternion operator splitting.
- The newly proposed method is applied to color image cross-channel restoration. Their efficiency and superiority are indicated by numerical results in terms of visual, PSNR, SSIM, MSE and CIEde2000 criteria. The numerical results also support the assertion that the proposed new methods can better preserve the color fidelity and texture.

The structure of this paper is as follows. We review several preliminary findings of the quaternion and SVTV regularization models in Section II of this paper. In Section III, we propose a new color image restoration model with an SVTV-CTV balance regularization term and give theoretical proof of the existence and uniqueness of the model solution. In Section IV, we propose an effective algorithm for the cross-channel SVTV-CTV balance regularization model. In Section V, we demonstrate numerical examples to illustrate the superiority of the proposed methods. In Section VI, we present concluding remarks.

II. PRELIMINARIES

In this section, we shortly recall quaternions and the existing total variation regularization functions for color images.

Let $\mathbb{Q} = \{\mathbf{a} = a_0 + a_1\mathbf{i} + a_2\mathbf{j} + a_3\mathbf{k} | a_0, a_1, a_2, a_3 \in \mathbb{R}\}$ denote the quaternion skew-field, \mathbb{Q}^n the set of n -dimensional quaternion vectors, and $\mathbb{Q}^{m \times n}$ the set of $m \times n$ quaternion matrices [15], where three imaginary units $\mathbf{i}, \mathbf{j}, \mathbf{k}$ satisfy

$$\mathbf{i}^2 = \mathbf{j}^2 = \mathbf{k}^2 = \mathbf{ijk} = -1.$$

For a quaternion $\mathbf{a} = a_0 + a_1\mathbf{i} + a_2\mathbf{j} + a_3\mathbf{k} \in \mathbb{Q}$, a_0 is called real part and a_1, a_2, a_3 are called three imaginary parts. Pure quaternion is nonzero quaternion with zero real part. The conjugate and modulus of \mathbf{a} are defined by $\bar{\mathbf{a}} = a_0 - a_1\mathbf{i} - a_2\mathbf{j} - a_3\mathbf{k}$ and $|\mathbf{a}| = \sqrt{\mathbf{a}\bar{\mathbf{a}}} = \sqrt{a_0^2 + a_1^2 + a_2^2 + a_3^2}$, respectively. Every nonzero quaternion is invertible and its unique inverse is defined by $\mathbf{a}^{-1} = \bar{\mathbf{a}}/|\mathbf{a}|^2$. The conjugate transpose of quaternion vector $\mathbf{v} = v_0 + v_1\mathbf{i} + v_2\mathbf{j} + v_3\mathbf{k} \in \mathbb{Q}^n$ is defined as $\mathbf{v}^* = v_0^T - v_1^T\mathbf{i} - v_2^T\mathbf{j} - v_3^T\mathbf{k}$, where $v_0, v_1, v_2, v_3 \in \mathbb{R}^n$ and \cdot^T denotes the transpose operator. Similarly, the conjugate transpose of quaternion matrix $\mathbf{A} = A_0 + A_1\mathbf{i} + A_2\mathbf{j} + A_3\mathbf{k} \in \mathbb{Q}^{m \times n}$ is defined as $\mathbf{A}^* = A_0^T - A_1^T\mathbf{i} - A_2^T\mathbf{j} - A_3^T\mathbf{k}$, where $A_0, A_1, A_2, A_3 \in \mathbb{R}^{m \times n}$. According to [22], we define a homeomorphic mapping \mathfrak{R} from quaternion matrices, vectors, scalars or functions to real structured real matrices:

$$\mathfrak{R}(\mathbf{A}) = \begin{bmatrix} A_0 & -A_1 & -A_2 & -A_3 \\ A_1 & A_0 & -A_3 & A_2 \\ A_2 & A_3 & A_0 & -A_1 \\ A_3 & -A_2 & A_1 & A_0 \end{bmatrix}. \quad (2)$$

Let $\mathfrak{R}_c(\mathbf{A})$ denote the first column of $\mathfrak{R}(\mathbf{A})$.

Now we introduce the measurement of quaternion vectors and matrices. The absolute of quaternion vector $\mathbf{v} = [\mathbf{v}_i] \in \mathbb{Q}^n$

is $|\mathbf{v}| = [|\mathbf{v}_i|] \in \mathbb{R}^n$. Similarly, the absolute of quaternion matrix $\mathbf{A} = [\mathbf{a}_{ij}] \in \mathbb{Q}^{m \times n}$ is $|\mathbf{A}| = [|\mathbf{a}_{ij}|] \in \mathbb{R}^{m \times n}$. From [20], we know that quaternion vector (or matrix) norms are functions from quaternion vectors (or matrices) to nonnegative real numbers.

Definition 1. Let $p \geq 1$. The p -norm of $\mathbf{v} \in \mathbb{Q}^n$ is $\|\mathbf{v}\|_p = (\sum_{i=1}^n |\mathbf{v}_i|^p)^{\frac{1}{p}}$. The p -norm and F -norm of $\mathbf{A} \in \mathbb{Q}^{m \times n}$ are

$$\|\mathbf{A}\|_p = \max_{\mathbf{x} \in \mathbb{Q}^n / \{0\}} \frac{\|\mathbf{Ax}\|_p}{\|\mathbf{x}\|_p}, \quad \|\mathbf{A}\|_F = \left(\sum_{i=1}^n \sum_{j=1}^n |\mathbf{a}_{ij}|^2 \right)^{\frac{1}{2}}.$$

From this definition and the definition (2), one can easily derive that $\|\mathbf{v}\|_2 = \|\Re_c(\mathbf{v})\|_2 = \frac{1}{2} \|\Re(\mathbf{v})\|_2$, $\|\mathbf{A}\|_2 = \|\Re(\mathbf{A})\|_2$ and $\|\mathbf{A}\|_F = \|\Re_c(\mathbf{A})\|_F = \frac{1}{2} \|\Re(\mathbf{A})\|_F$.

Next, we give a brief description of the SVTV regularization function for color image based on quaternion representation [21]. A quaternion function

$$\mathbf{u}(x, y) = u_1(x, y)\mathbf{i} + u_2(x, y)\mathbf{j} + u_3(x, y)\mathbf{k}$$

was used to represent a color image in the RGB color space in [21], where (x, y) denotes the position of a color pixel in a given range Ω and three real binary functions $u_i(x, y)$ ($i = 1, 2, 3$) denote pixel values of red, green and blue channels, respectively. After a strict derivation of quaternion operations, a real-valued version of SVTV was also given in [21], which make it possible to handle it by real calculations instead of quaternion calculations. For simplicity, let $\partial_{x/y}$ denote ∂_x or ∂_y . Without causing misunderstandings, we still use the following vector function to represent a color image,

$$\mathbf{u}(x, y) := [u_1(x, y) \quad u_2(x, y) \quad u_3(x, y)]^T. \quad (3)$$

Define

$$\partial_{x/y}\mathbf{u}(x, y)^T = \begin{bmatrix} \partial_{x/y}u_1(x, y) \\ \partial_{x/y}u_2(x, y) \\ \partial_{x/y}u_3(x, y) \end{bmatrix}, \quad C = \begin{bmatrix} 2 & -1 & -1 \\ -1 & 2 & -1 \\ -1 & -1 & 2 \end{bmatrix}.$$

The saturation and value components of color image $\mathbf{u}(x, y)$ are defined as

$$|\mathbf{u}(x, y)|_s = \frac{1}{2} \|C\mathbf{u}(x, y)^T\|_2,$$

$$|\mathbf{u}(x, y)|_v = \frac{1}{\sqrt{3}} \left| \sum_{i=1}^3 u_i(x, y) \right|.$$

The SVTV regularization is defined in [21] by

$$\begin{aligned} \text{SVTV}(\mathbf{u}) &= \int_{\Omega} \sqrt{(|\partial_x \mathbf{u}(x, y)|_s^2) + (|\partial_y \mathbf{u}(x, y)|_s^2)} dx dy \\ &\quad + \alpha \sqrt{(|\partial_x \mathbf{u}(x, y)|_v^2) + (|\partial_y \mathbf{u}(x, y)|_v^2)} dx dy, \end{aligned} \quad (4)$$

where α is the weight of the value component. $\text{SVTV}(\mathbf{u})$ is exactly a functional of real functions: $u_1(x, y)$, $u_2(x, y)$, $u_3(x, y)$.

Before SVTV regularization, there are several well-known TV regularizations developed for color image in the RGB color space. For instance,

- Blomgren and Chan [1]:

$$\text{CTV}_1(\mathbf{u}) := \sqrt{\sum_{i=1}^3 \left(\int_{\Omega} \|\nabla u_i(x, y)\|_2 dx dy \right)^2}. \quad (5)$$

- Bresson and Chan [2]:

$$\text{CTV}_2(\mathbf{u}) := \int_{\Omega} \sqrt{\sum_{k=1}^3 \|\nabla u_k(x, y)\|_2^2} dx dy. \quad (6)$$

- Sapiro [27]:

$$\text{VTV}(\mathbf{u}) := \int_{\Omega} f(\lambda((\nabla \mathbf{u}(x, y))^T \nabla \mathbf{u}(x, y))) dx dy, \quad (7)$$

where $\lambda(\cdot)$ refers to eigenvalues and $f(\cdot)$ is a penalty function on eigenvalues.

In above equations, $\nabla = [\partial_x, \partial_y]^T$ represents the gradient operator. In [6], classic and advanced versions of vector TV regularizations are summarized into a classification called collaborative total variation (CTV). When applied to color images, they are all based on one color space. A new regularization on different color spaces will be introduced in next section.

III. CROSS-SPACE COLOR IMAGE RESTORATION MODEL

In this section, we present a novel cross color space regularization and a new color image restoration model for cross-channel deblurring.

With the degradation model (1) in hand, we are concerned with a general framework for color image restoration expressed as

$$\min_{\substack{\boldsymbol{\lambda} \in \mathbb{R}^m \\ \mathbf{u}(x, y) \in \mathbb{BV}(\Omega)}} J(\mathbf{u}, \boldsymbol{\lambda}) + F(\mathbf{u}, \mathbf{z}, \mathbf{K}), \quad (8)$$

where \mathbb{R}^m denotes the m -dimensional real-valued vector space, $\mathbb{BV}(\Omega) = \{\mathbf{u}(x, y) = u_1(x, y)\mathbf{i} + u_2(x, y)\mathbf{j} + u_3(x, y)\mathbf{k} \mid u_i(x, y) \in \text{BV}(\Omega), (x, y) \in \Omega\}$ and $\text{BV}(\Omega)$ is bounded variation space on a given color image region $\Omega \subseteq \mathbb{R}^2$. The function $J(\mathbf{u}, \boldsymbol{\lambda})$ punishes the gradients of the targeted color image $\mathbf{u}(x, y)$ in different color spaces and it is called a cross color space regularization term with balance parameters $\boldsymbol{\lambda} = (\lambda_1, \lambda_2, \dots, \lambda_m) \in \mathbb{R}^m$. The function $F(\mathbf{u}, \mathbf{z}, \mathbf{K})$ is a data fidelity term to control the distance between the targeted and observed color images under the blurring operator.

We now face two difficulties: how to construct the correct regularization term, and how to use quaternion matrices to approximate blurring operators. Next, let us do a detailed analysis.

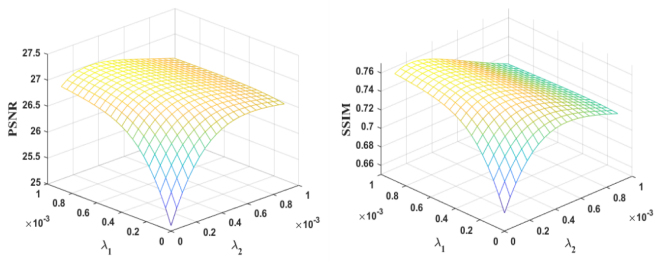
A. Cross color space regularization term

The regularization term $J(\mathbf{u}, \boldsymbol{\lambda})$ is a fusion of regularizations on different color spaces. This fusion is tailored to extract information across various dimensions within color images, thereby enhancing the preservation of color and texture details. For instance, a regularization crossing HSV and RGB color spaces can be defined by

$$J(\mathbf{u}, \boldsymbol{\lambda}) = \lambda_1 \text{SVTV}(\mathbf{u}) + \lambda_2 \text{CTV}(\mathbf{u}), \quad (9)$$

where regularization function SSVTV is defined in (4), CTV represents CTV₁ or CTV₂ defined in (5) and (6), and $\lambda_1, \lambda_2 \in \mathbb{R}$. The choice of different regularization functions is empirical and it relies on the requirement from practical applications. A solution based on machine learning methods is to perform a linear combination of all possible regular functions with parameters, and then learn the best parameters. There are a number of well-known techniques for dynamically calculating optimal parameters, such as the generalized cross-validation [11], [16], the L-curve method [14] and the discrepancy principle [29]. Here, we generalize the L-curve method to a new L-surface method to determine optimal parameters simultaneously.

The L-surface method is to find a sweet spot on a surface with respect to a certain quality index of the parameter λ . To be clear, we describe the L-surface method by applying it to determine the optimal $\lambda = (\lambda_1, \lambda_2)$ in (9). Suppose we have obtained an observed color image, say 'statues' in Figure 5, under the setting of Example V-A. The upper bound of parameters is set as $b = 2\sqrt{N\sigma^2} \times 10^{-3}$, where N is image size and σ is the noise level. The surface of PSNR values of restored color images are plotted in Figure 1 (a) according to $\lambda_1, \lambda_2 \in (0, b)$. High PSNR values are obtained with $\lambda_1 \in (0.4 \times 10^{-3}, b)$ and $\lambda_2 \in (0.2 \times 10^{-3}, 0.5 \times 10^{-3})$ and the highest PSNR value is 27.1903 at $(\lambda_1 = 0.8 \times 10^{-3}, \lambda_2 = 0.2 \times 10^{-3})$. The surface of SSIM values of restored color images are plotted in Figure 1 (b) according to $\lambda_1, \lambda_2 \in (0, b)$. High SSIM values are obtained with $\lambda_1 \in (0.5 \times 10^{-3}, b)$ and $\lambda_2 \in (0.1 \times 10^{-3}, 0.3 \times 10^{-3})$, and the highest SSIM value is 0.7704 at $(\lambda_1 = 0.8 \times 10^{-3}, \lambda_2 = 0.1 \times 10^{-3})$. By the weighted average surface of above PSNR and SSIM surfaces, we obtain the sweet spot $\lambda = (0.8 \times 10^{-3}, 0.2 \times 10^{-3})$ that leads to a good combination of SSVTV and CTV regularizations.



(a) PSNR values in relation to λ_1, λ_2 . (b) SSIM values in relation to λ_1, λ_2 .

Fig. 1. The values of PSNR and SSIM for the restored image 'statues' in different λ_1, λ_2 conditions.

Obviously, the combined regularization term $J(\mathbf{u}, \lambda)$ performs better than single regularization SSVTV(\mathbf{u}) or CTV(\mathbf{u}). This implies that the color image restoration model (8) with the combined regularization term can obtain a broader range of pre-existing knowledge about color image and thus it is enriched an ability to interpret color image. To demonstrate the superiority, we plot the PSNR and SSIM values in Figure 2 at boundary $\lambda_1 = 0$ or $\lambda_2 = 0$. We can see that the

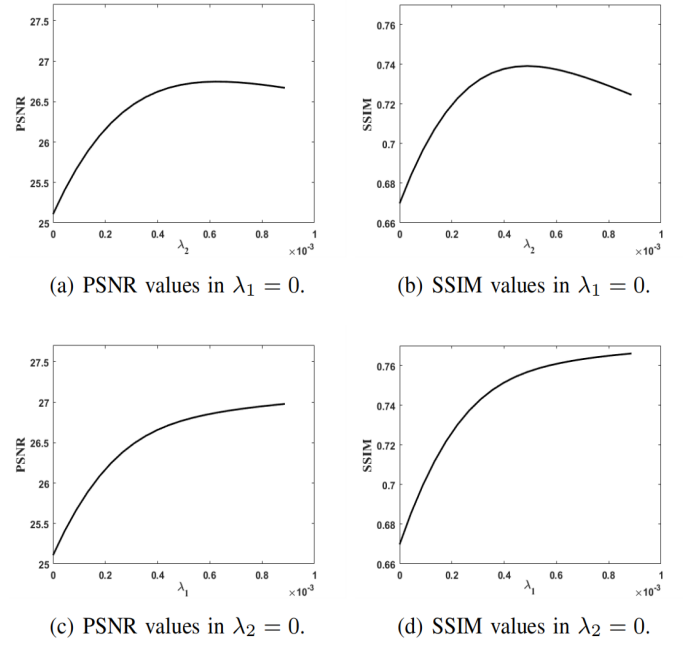


Fig. 2. The values of PSNR and SSIM for the restored image 'statues' in $\lambda_1 = 0$ or $\lambda_2 = 0$.

PSNR and SSIM values in Figure 2 are significantly smaller than 27.1903 and 0.7704, respectively. So one can conclude that color image restoration models with cross color space regularization performs better than those with single color space regularization.

B. Fidelity term with quaternion operator

The fidelity term $F(\mathbf{u}, \mathbf{z}, \mathbf{K})$ of color image restoration model (8) aims to minimize the distance between the observed color image \mathbf{z} and the original color image \mathbf{u} after a blurring operation. Next, we introduce a new description of blur operator by quaternion operator. The new form can lead to a stable algorithm to compute a solution without color confusion and mutual infection.

At first, we recall the cross-channel blur mechanism. The color image cross-channel blurring process is mathematically described in [9], [10], [12] as

$$\hat{\mathbf{u}}(x, y) = \mathbf{K} \star \mathbf{u}(x, y), \quad (10)$$

where $\mathbf{K} = W \odot K$ with

$$K = \begin{bmatrix} K_{11} & K_{12} & K_{13} \\ K_{21} & K_{22} & K_{23} \\ K_{31} & K_{32} & K_{33} \end{bmatrix}, \quad W = \begin{bmatrix} w_{11} & w_{12} & w_{13} \\ w_{21} & w_{22} & w_{23} \\ w_{31} & w_{32} & w_{33} \end{bmatrix}. \quad (11)$$

In (11), the sub-matrices of K , denoted by K_{ij} 's, are real blur kernels, and the entries of W , w_{ij} 's, belong to the interval $[0, 1]$ and $\sum_{j=1}^3 w_{ij} = 1$ for $i = 1, 2, 3$.

The cross-channel blurring process (10) can be embedded into a higher dimensional space,

$$\begin{bmatrix} \hat{u}_0(x, y) \\ \hat{u}_r(x, y) \\ \hat{u}_g(x, y) \\ \hat{u}_b(x, y) \end{bmatrix} = \begin{bmatrix} B_{11} & B_{12} & B_{13} & B_{14} \\ B_{21} & \mathbf{K} & & \\ B_{31} & & & \\ B_{41} & & & \end{bmatrix} \star \begin{bmatrix} u_0(x, y) \\ u_1(x, y) \\ u_2(x, y) \\ u_3(x, y) \end{bmatrix}, \quad (12)$$

where $\hat{u}_0(x, y)$ and $u_0(x, y)$ are zero functions and B_{ij} 's are arbitrary operators of the same size of K_{ij} 's in (11). Denote the extended blurring operator by B , that is,

$$B = \begin{bmatrix} B_{11} & B_{12} & B_{13} & B_{14} \\ B_{21} & \mathbf{K} & & \\ B_{31} & & & \\ B_{41} & & & \end{bmatrix}. \quad (13)$$

It can be splitted into a sum of a JRS-symmetric matrix Q and a 4×4 real block matrix R , according to the following rules:

$$B = Q + R, \quad (14)$$

where

$$\begin{aligned} Q &= \frac{1}{4}(B + J_n B J_n^T + R_n B R_n^T + S_n B S_n^T), \\ R &= \frac{1}{4}(3B - J_n B J_n^T - R_n B R_n^T - S_n B S_n^T), \end{aligned} \quad (15)$$

and J_n, R_n, S_n are unitary operators defined in [24]. Since these unitary operators satisfy $J_n J_n = -I_{4n}$, $J_n R_n = S_n$ and $J_n S_n = -R_n$, we can easily derive

$$J_n Q J_n^T = Q, \quad R_n Q R_n^T = Q, \quad S_n Q S_n^T = Q.$$

From [24], there exists a quaternion matrix

$$\mathbf{Q} = Q_0 + Q_1 \mathbf{i} + Q_2 \mathbf{j} + Q_3 \mathbf{k} \quad (16)$$

such that

$$Q = \Re(\mathbf{Q}), \quad (17)$$

and

$$\begin{aligned} Q_0 &= \frac{1}{4}(B_{11} + w_{11} K_{11} + w_{22} K_{22} + w_{33} K_{33}), \\ Q_1 &= \frac{1}{4}(B_{21} - B_{12} + w_{32} K_{32} - w_{23} K_{23}), \\ Q_2 &= \frac{1}{4}(B_{31} - B_{13} + w_{13} K_{13} - w_{31} K_{31}), \\ Q_3 &= \frac{1}{4}(B_{41} - B_{14} + w_{21} K_{21} - w_{12} K_{12}). \end{aligned} \quad (18)$$

Note that the blocks B_{ij} 's of matrix B defined by (13) are solution of the minimization problem:

$$\begin{aligned} \min_{B_{ij}} \|B - Q\|_F \\ \text{s.t. } B_{12} \star u_1 + B_{1,3} \star u_2 + B_{14} \star u_3 = 0. \end{aligned} \quad (19)$$

Now we introduce a quaternion representation of blurring process. Define

$$\hat{\mathbf{u}}(x, y) = \hat{u}_0(x, y) + \hat{u}_r(x, y)\mathbf{i} + \hat{u}_g(x, y)\mathbf{j} + \hat{u}_b(x, y)\mathbf{k},$$

$$\mathbf{u}(x, y) = u_0(x, y) + u_r(x, y)\mathbf{i} + u_g(x, y)\mathbf{j} + u_b(x, y)\mathbf{k}.$$

Based on the above matrix splitting, the blurring process (12) can be rewritten as

$$\hat{\mathbf{u}}(x, y) = \mathbf{Q} \star \mathbf{u}(x, y) + \mathbf{r}(x, y), \quad (20)$$

where

$$\begin{aligned} \mathbf{r}(x, y) &= r_0(x, y) + r_1(x, y)\mathbf{i} + r_2(x, y)\mathbf{j} + r_3(x, y)\mathbf{k}, \\ \begin{bmatrix} r_0(x, y) \\ r_1(x, y) \\ r_2(x, y) \\ r_3(x, y) \end{bmatrix} &= R \star \begin{bmatrix} u_0(x, y) \\ u_1(x, y) \\ u_2(x, y) \\ u_3(x, y) \end{bmatrix}. \end{aligned}$$

In the discrete form, the cross-channel blurring process is in fact a sum of a quaternion matrix-vector product \mathbf{Qu} and a quaternion vector \mathbf{r} . The quaternion operations can preserve the ratio of red, green and blue information of color pixels in the blurring process and thus, color confusion and interinfection can be reduced in the delurring process. As a result, the correlation of color channels are well preserved and the recovered color images can achieve a high quality. In the paper, there always exists an invertible quaternion matrix \mathbf{Q} such that $\mathbf{Qu} = \hat{\mathbf{u}}$. However, it is impractical to compute such quaternion matrix, since a large number of pairs of original and observed color images under the same blurring process are in need. Especially, the original color image is definitely unknown. So we alternatively construct \mathbf{Q} according to (16), (18) and (19) to minimize $\|\mathbf{r}\|_2$ in this paper.

Let us turn back to construct the fidelity term $F(\mathbf{u}, \mathbf{z}, \mathbf{K})$ of color image restoration model (8). To treat different kinds of noise, we define the distance between the observed and original color images by L_p norm as

$$F(\mathbf{u}, \mathbf{z}, \mathbf{K}) = \frac{1}{p} \int_{\Omega} |\mathbf{K} \star \mathbf{u}(x, y) - \mathbf{z}(x, y)|^p dx dy, \quad p \geq 1. \quad (21)$$

According to (10) and (20), we have a quaternion operator form

$$F(\mathbf{u}, \mathbf{z}, \mathbf{K}) = \frac{1}{p} \int_{\Omega} |\mathbf{Q} \star \mathbf{u}(x, y) + \mathbf{r}(x, y) - \mathbf{z}(x, y)|^p dx dy. \quad (22)$$

This general framework offers a flexibility to adaptively choose suitable fidelity terms to restore color images based on specific noise types and image texture characteristics. For instance, one can explore the utilization of the L_2 fidelity term to reduce Gaussian noise, the L_1 fidelity term to eliminate Poisson and mixed noise, and the L_1-L_2 mixed fidelity term for more effectively mitigating losses induced by degradation factors. The forms in (21) and (22) are mathematically equivalent to each other. The former is used for theoretical analysis and the latter is used to design stable and fast algorithm.

C. A new color image restoration model

Now we propose a color image restoration model with a cross color space regularization term and a fidelity with quaternion operator. To make the description clear, we concentrate into two color spaces: the widely used RGB color space and the more human eye-perceiving HSV color space.

Let the cross-space regularization be defined as in (9) and the fidelity term in (22). For an observed image \mathbf{z} , a new cross-space color image restoration model is

$$\begin{aligned} \hat{\mathbf{u}} = \arg \min_{\mathbf{u}(x, y) \in \mathbb{BV}(\Omega)} \lambda_1 \text{SVTV}(\mathbf{u}) + \lambda_2 \text{CTV}(\mathbf{u}) + \\ \frac{1}{p} \int_{\Omega} |\mathbf{Q} \star \mathbf{u} + \mathbf{r} - \mathbf{z}|^p dx dy, \end{aligned} \quad (23)$$

where λ_1 and λ_2 are two given nonnegative regularization parameters, and p is a positive integer not less than 1. Here, parameters λ_1 and λ_2 play in two roles: one is the regularization parameters to banlance regularization and fidelity terms, and another is the balance parameters between two regularization terms.

This model contains one fidelity term and two regularization terms: SVTV regularization and CTV regularization. The two regularizations complement each other with color and texture information. In this way, the loss of information caused by considering only one color space will be decreased. Parameters λ_1 and λ_2 control the balance of them. When $\lambda_1 = 0$, the model degenerates to the classical color total variation model; when $\lambda_2 = 0$, the model degenerates to the saturation value total variation model; and when both λ_1 and λ_2 are greater than 0, both regularization terms come into play and the information of saturation, value, red, green and blue is used for color image restoration.

Next, we analyze the solvability of the newly proposed model (23) with $p = 2$.

Theorem 1. *If $p = 2$, there is at least one solution for the minimization problem (23) and moreover, the solution is unique when $\mathbf{u} \mapsto \mathbf{Q} \star \mathbf{u} + \mathbf{r}$ is injective.*

Proof: If $\mathbf{u}(x, y)$ is a constant value function, then $\text{SVTV}(\mathbf{u}) = 0$ and $\text{CTV}(\mathbf{u}) = 0$. The energy in (7) thus becomes finite. This implies that the infimum of the energy must be finite. Suppose that $\{\mathbf{u}^{(n)}(x, y)\}$ is a minimizing sequence of problem (7). Consequently, a constant $M > 0$ exists such that

$$\text{SVTV}(\mathbf{u}^{(n)}) \leq M.$$

We get that $\left\{ \text{SVTV}(\mathbf{u}^{(n)}) + \sum_{i=1}^3 \|u_i^{(n)}\|_{L^1} \right\}$ is uniformly bounded by combining the boundedness of $u_1^{(n)}, u_2^{(n)}, u_3^{(n)}$. Noting the compactness of [21], we know that there exist u_1^*, u_2^*, u_3^* such that

$$u_i^{(n)}(x, y) \xrightarrow{L^1(\Omega)} u_i^*(x, y), \quad u_i^{(n)}(x, y) \rightarrow u_i^*(x, y) \quad \text{a.e. } (x, y) \in \Omega, \quad i = 1, 2, 3.$$

Recall that $\mathbf{Q} \star \mathbf{u}(x, y) + \mathbf{r}(x, y) = \mathbf{K} \star \mathbf{u}(x, y)$. Subsequently, the convergence of the following results is valid:

$$(\mathbf{K} \star u_i^{(n)}(x, y) - z_i(x, y))^2 \rightarrow (\mathbf{K} \star u_i^*(x, y) - z_i(x, y))^2 \quad \text{a.e. } (x, y) \in \Omega, \quad i = 1, 2, 3.$$

Taking advantage of the Fatou's lemma, one has

$$\begin{aligned} & \sum_{i=1}^3 \liminf \int_{\Omega} (\mathbf{K} \star u_i^{(n)}(x, y) - z_i(x, y))^2 dx dy \\ & \geq \sum_{i=1}^3 \int_{\Omega} (\mathbf{K} \star u_i^*(x, y) - z_i(x, y))^2 dx dy. \end{aligned}$$

On account of the lower semicontinuity of $\text{CTV}(\mathbf{u})$ and $\text{SVTV}(\mathbf{u})$,

$$\begin{aligned} \liminf \text{CTV}(\mathbf{u}^{(n)}) & \geq \text{CTV}(\mathbf{u}^*), \\ \liminf \text{SVTV}(\mathbf{u}^{(n)}) & \geq \text{SVTV}(\mathbf{u}^*), \end{aligned}$$

then we obtain

$$\begin{aligned} & \liminf (\lambda_1 \text{SVTV}(\mathbf{u}^{(n)}) + \lambda_2 \text{CTV}(\mathbf{u}^{(n)})) \\ & + \sum_{i=1}^3 \int_{\Omega} (\mathbf{K} \star u_i^{(n)}(x, y) - z_i(x, y))^2 dx dy \\ & \geq \lambda_1 \text{SVTV}(\mathbf{u}^*) + \lambda_2 \text{CTV}(\mathbf{u}^*) \\ & + \sum_{i=1}^3 \int_{\Omega} (\mathbf{K} \star u_i^*(x, y) - z_i(x, y))^2 dx dy. \end{aligned}$$

It leads to the existence of the solution of (7) in the main body. If $\mathbf{u} \mapsto \mathbf{Q} \star \mathbf{u} + \mathbf{r} (= \mathbf{K} \star \mathbf{u})$ is injective, the uniqueness of the solution can be obtained quickly by combining the convexity of $\text{SVTV}(\mathbf{u})$ and $\text{CTV}(\mathbf{u})$. \blacksquare

An important advantage of the newly proposed model (23) is that it takes into account the color channels coupling and the local smoothing within each channel. This implicitly leads to achieving better results in terms of both image texture and color fidelity. We can get the explanation from the corresponding Euler-Lagrange equation:

$$\begin{aligned} & \frac{\lambda_1}{3} \nabla \cdot \left(\frac{\nabla(\mathbf{Cu})}{\sqrt{(|\partial_x \mathbf{u}(x, y)|_s^2) + (|\partial_y \mathbf{u}(x, y)|_s^2)}} \right. \\ & \quad \left. + \alpha \frac{\nabla \mathbf{u}}{\sqrt{(|\partial_x \mathbf{u}(x, y)|_v^2) + (|\partial_y \mathbf{u}(x, y)|_v^2)}} \right) \\ & + \lambda_2 \sum_{i=1}^3 \nabla \cdot \left(\frac{\nabla u_i(x, y)}{|\mathbf{u}(x, y)|} \right) - (\mathbf{K}^* \star \mathbf{K} \star \mathbf{u} - \mathbf{K}^* \star \mathbf{z}) = 0. \end{aligned} \quad (24)$$

In (24), the proposed model takes into account both the diffusion coefficients of the channel coupling over the saturation and value components and the diffusion coefficients of the summation of the individual channels over the RGB space. The quaternion representation also leads to many other advantages, such as the values of three color channels of a color pixel are flocked together and their physical meanings are preserved in the whole color image processing based on quaternion computation. Especially, color distortion will be hugely reduced in the recovered color image by the new model.

To end this section, we present the dual form of model (23). The dual forms of regularization functions SVTV and CTV are

$$\begin{aligned} \text{SVTV}(\mathbf{u}) &= \max_{\|\mathbf{g}\| \leq 1} \langle \text{diag}(1, 1, \alpha) \mathbf{P} \mathbf{u}, \nabla \mathbf{g} \rangle, \\ \text{CTV}(\mathbf{u}) &= \max_{\|\mathbf{h}\| \leq 1} \langle \mathbf{u}, \nabla \mathbf{h} \rangle, \end{aligned}$$

where \mathbf{P} is an orthogonal transformation matrix that takes the form of

$$\mathbf{P} = \begin{bmatrix} \frac{1}{\sqrt{2}} I & \frac{-1}{\sqrt{2}} I & \mathbf{0} \\ \frac{1}{\sqrt{6}} I & \frac{1}{\sqrt{6}} I & \frac{-2}{\sqrt{6}} I \\ \frac{1}{\sqrt{3}} I & \frac{1}{\sqrt{3}} I & \frac{1}{\sqrt{3}} I \end{bmatrix}.$$

By converting the regularization terms into dual forms, we can rephrase the minimization problem (23) as the following dual form:

$$\begin{aligned} & \min_{\mathbf{u}} \max_{\substack{\|\mathbf{g}\| \leq 1 \\ \|\mathbf{h}\| \leq 1}} \lambda_1 \langle \text{diag}(1, 1, \alpha) \mathbf{P} \mathbf{u}, \nabla \mathbf{g} \rangle + \lambda_2 \langle \mathbf{u}, \nabla \mathbf{h} \rangle + \\ & \quad \frac{1}{2} \|\mathbf{Q} \star \mathbf{u} + \mathbf{r} - \mathbf{z}\|^2. \end{aligned} \quad (25)$$

In the dual form, the solution $\mathbf{u}(x, y)$ can be differentiable or not, which expands the feasible set. Obviously, the min-max problem (25) is a new saddle-point problem.

There are various methods to solve the new model (23) or the dual form (25) with real variables. However, there are no methods for solving them with quaternion variables. So we will develop fast algorithms for solving model (23) in next section.

IV. FAST ALGORITHMS

In this section, we present a new stable and fast algorithm for model (23) based on quaternion operator splitting.

It is impractical to solve the Euler-Lagrange equation (24) directly, since a non-linear differential equation leads to a non-linear system after discretization. So we introduce two auxiliary variables into (23) and obtain an mathematically equivalent model:

$$\begin{aligned} \hat{\mathbf{u}} = \arg \min_{\mathbf{u}} & \lambda_1 \text{SVTV}(\mathbf{w}) + \lambda_2 \text{CTV}(\mathbf{v}) + \\ & \frac{1}{2} \|\mathbf{Q} \star \mathbf{u} + \mathbf{r} - \mathbf{z}\|^2, \\ \text{s.t. } & \mathbf{w} = \mathbf{u}, \quad \mathbf{v} = \mathbf{u}. \end{aligned}$$

The constraints mentioned above can be converted into an unconstrained problem:

$$\begin{aligned} \hat{\mathbf{u}} = \arg \min_{\mathbf{u}, \mathbf{w}, \mathbf{v}} & \lambda_1 \text{SVTV}(\mathbf{w}) + \frac{\alpha_1}{2} \|\mathbf{w} - \mathbf{u}\|^2 + \\ & \frac{1}{2} \|\mathbf{Q} \star \mathbf{u} + \mathbf{r} - \mathbf{z}\|^2 + \lambda_2 \text{CTV}(\mathbf{v}) + \frac{\alpha_2}{2} \|\mathbf{v} - \mathbf{u}\|^2, \end{aligned} \quad (26)$$

where α_1 and α_2 are two positive parameters. Three unknown variables \mathbf{u} , \mathbf{w} and \mathbf{v} can be splitted into two independent groups and under the framework of alternating minimization method, problem (26) can be solved by alternatively solving two subproblems:

- **u-subproblem**

With fixing \mathbf{w} and \mathbf{v} , the minimization problem (26) is equivalently reduced to

$$\begin{aligned} \arg \min_{\mathbf{u}} & \frac{\alpha_1}{2} \|\mathbf{u} - \mathbf{w}\|^2 + \frac{\alpha_2}{2} \|\mathbf{u} - \mathbf{v}\|^2 + \\ & \frac{1}{2} \|\mathbf{Q} \star \mathbf{u} + \mathbf{r} - \mathbf{z}\|^2. \end{aligned} \quad (27)$$

- **(w, v)-subproblem**

With fixing \mathbf{u} , the minimization problem (26) is equivalently reduced to

$$\begin{aligned} \arg \min_{\mathbf{w}, \mathbf{v}} & \lambda_1 \text{SVTV}(\mathbf{w}) + \frac{\alpha_1}{2} \|\mathbf{w} - \mathbf{u}\|^2 + \\ & \lambda_2 \text{CTV}(\mathbf{v}) + \frac{\alpha_2}{2} \|\mathbf{v} - \mathbf{u}\|^2. \end{aligned} \quad (28)$$

A. Quaternion operator splitting method for u-subproblem

Now we consider the \mathbf{u} -subproblem (27) and use its real presentation to introduce a quaternion operator splitting method.

From the analysis in Section III-B, the real representation of (27) is

$$\begin{aligned} \arg \min_{\mathbf{u}} & \frac{\alpha_1}{2} \|\mathbf{u} - \mathbf{w}\|^2 + \frac{\alpha_2}{2} \|\mathbf{u} - \mathbf{v}\|^2 + \\ & \frac{1}{2} \|\mathbf{B}\mathbf{u} - \mathbf{z}\|^2, \end{aligned} \quad (29)$$

where $\mathbf{B} = \mathbf{Q} + \mathbf{R}$ with \mathbf{Q} and \mathbf{R} being 4-by-4 block matrices defined by (15). Its nominal equation is

$$[\mathbf{B}^T \mathbf{B} + (\alpha_1 + \alpha_2) \mathbf{I}] \mathbf{u} = \mathbf{B}^T \mathbf{z} + \alpha_1 \mathbf{w} + \alpha_2 \mathbf{v}. \quad (30)$$

We split $\mathbf{B}^T \mathbf{B}$ into $\mathbf{Q}^T \mathbf{Q} + \mathbf{Q}^T \mathbf{R} + \mathbf{R}^T \mathbf{Q} + \mathbf{R}^T \mathbf{R}$ and obtain an iterative format

$$\begin{aligned} [\mathbf{Q}^T \mathbf{Q} + (\alpha_1 + \alpha_2) \mathbf{I}] \mathbf{u}^{k+1} = & -(\mathbf{Q}^T \mathbf{R} + \mathbf{R}^T \mathbf{Q} + \mathbf{R}^T \mathbf{R}) \mathbf{u}^k \\ & + \lambda(\mathbf{Q} + \mathbf{R})^T \mathbf{z} + \alpha_1 \mathbf{w} + \alpha_2 \mathbf{v}. \end{aligned} \quad (31)$$

From the structure of \mathbf{Q} as in (17), we can construct a equivalent quaternion linear system

$$\mathbf{A} \mathbf{u}^{k+1} = \mathbf{b}, \quad (32)$$

where $\mathbf{A} = \mathbf{A}_0 + \mathbf{A}_1 \mathbf{i} + \mathbf{A}_2 \mathbf{j} + \mathbf{A}_3 \mathbf{k}$ with $\Re(\mathbf{A}) = \mathbf{Q}^T \mathbf{Q} + \alpha_1 \mathbf{I} + \alpha_2 \mathbf{I}$ and $\mathbf{b} = \mathbf{b}_0 + \mathbf{b}_1 \mathbf{i} + \mathbf{b}_2 \mathbf{j} + \mathbf{b}_3 \mathbf{k}$ with $\Re_c(\mathbf{b})$ denotes the right handside of (31). So the solution of the \mathbf{u} -subproblem (27) can be computed by iteratively solving (32).

In the above, we have proposed a quaternion operator splitting method for solving the \mathbf{u} -subproblem, where the coefficient matrix is splitted into a quaternion operator and a residual operator. This leads to an advantage that the color information of restored color image \mathbf{u} is preserved by quaternion algebra operations in the solving process. This advantage will be verified numerically in Section V. Now the core work becomes solving (32). Obviously, the QGMRES method proposed in [22] is feasible to solve this quaternion linear system. However, we can further apply the Hermitian and positive definite properties of \mathbf{A} to develop a new quaternion conjugate gradient method. Inspired by [22], we present a structure-preserving version in Algorithm 1. The quaternion matrix-vector product is implemented by real operation, i.e., $\mathbf{Ax}_k = \Re^{-1}(\Re(\mathbf{A})\Re(\mathbf{x}_k))$.

Algorithm 1 Quaternion Conjugate Gradient Method

- 1: **Initialization** Set the stopping criteria $tol > 0$ and the initial solution $\mathbf{x}_0 = 0$.
- 2: $k = 0$, $\mathbf{r}_k = \mathbf{b} - \Re^{-1}(\Re(\mathbf{A})\Re(\mathbf{x}_k))$ and let $\mathbf{p}_k = \mathbf{r}_k$.
- 3: **while** $\|\Re_c(\mathbf{r}_k)\|_2 > tol$ **do**
- 4: $\mathbf{q}_k = \Re^{-1}(\Re(\mathbf{A})\Re(\mathbf{p}_k))$,
- 5: Compute $a_k = \frac{\langle \mathbf{r}_k, \mathbf{r}_k \rangle}{\langle \mathbf{p}_k, \mathbf{q}_k \rangle}$,
- 6: Compute $\mathbf{x}_{k+1} = \mathbf{x}_k + a_k \mathbf{p}_k$,
- 7: Compute $\mathbf{r}_{k+1} = \mathbf{r}_k + a_k \mathbf{q}_k$,
- 8: Compute $b_k = \frac{\langle \mathbf{r}_{k+1}, \mathbf{r}_{k+1} \rangle}{\langle \mathbf{r}_k, \mathbf{r}_k \rangle}$,
- 9: Compute $\mathbf{p}_{k+1} = \mathbf{r}_{k+1} + b_k \mathbf{p}_k$,
- 10: $k = k + 1$.
- 11: **end while**

B. Augmented Lagrangian method for (w, v)-subproblem

Now, we present a new augmented Lagrangian method for solving (\mathbf{w}, \mathbf{v}) -subproblem (28). Since the two variables are independent of each other and have no intersecting terms, we construct the augmented Lagrangian schemes of computing \mathbf{w} and \mathbf{v} , respectively.

- **w-subproblem**

With \mathbf{u} and \mathbf{v} fixed, the minimization problem (28) is reduced to

$$\arg \min_{\mathbf{w}} \lambda_1 \text{SVTV}(\mathbf{w}) + \frac{\alpha_1}{2} \|\mathbf{w} - \mathbf{u}\|^2. \quad (33)$$

We define two discrete differential operators $\mathbf{D}_x, \mathbf{D}_y$,

$$\begin{aligned} (\mathbf{D}_x \mathbf{w})_{i,j} &= \mathbf{w}(i,j) - \mathbf{w}(i-1,j), \\ (\mathbf{D}_y \mathbf{w})_{i,j} &= \mathbf{w}(i,j) - \mathbf{w}(i,j-1), \end{aligned}$$

under adequate boundary conditions for color image. Define

$$\mathbf{s} = \mathbf{P}\mathbf{w} \text{ and } \mathbf{q} = \mathbf{P}\mathbf{u}.$$

Then the objective color image restoration model (33) is reformulated as

$$\begin{aligned} \arg \min_{\mathbf{s}} \frac{\lambda_1}{\alpha_1} \sum_{i=1}^m \sum_{j=1}^n \left(\sqrt{\sum_{k=1}^2 ((\mathbf{D}_x s_k)_{ij})^2 + ((\mathbf{D}_y s_k)_{ij})^2} \right. \\ \left. + \alpha \sqrt{((\mathbf{D}_x s_3)_{ij})^2 + ((\mathbf{D}_y s_3)_{ij})^2} \right) + \frac{1}{2} \|\mathbf{s} - \mathbf{q}\|^2. \end{aligned} \quad (34)$$

By introducing auxiliary variables t_i^x and t_i^y , the minimization problem (34) is equivalently rewritten into

$$\begin{aligned} \arg \min_{\mathbf{s}} \frac{\lambda_1}{\alpha_1} \sum_{i=1}^m \sum_{j=1}^n \left(\sqrt{\sum_{k=1}^2 |(t_k^x)_{ij}|^2 + |(t_k^y)_{ij}|^2} \right. \\ \left. + \alpha \sqrt{|(t_3^x)_{ij}|^2 + |(t_3^y)_{ij}|^2} \right) + \frac{1}{2} \|\mathbf{s} - \mathbf{q}\|^2, \\ \text{s.t. } t_1^x = \mathbf{D}_x s_1, t_2^x = \mathbf{D}_x s_2, t_3^x = \mathbf{D}_x s_3, \\ t_1^y = \mathbf{D}_y s_1, t_2^y = \mathbf{D}_y s_2, t_3^y = \mathbf{D}_y s_3. \end{aligned}$$

The augmented Lagrangian of the aforementioned minimization problem is

$$\begin{aligned} \frac{\lambda_1}{\alpha_1} \sum_{i=1}^m \sum_{j=1}^n \left(\sqrt{\sum_{k=1}^2 |(t_k^x)_{ij}|^2 + |(t_k^y)_{ij}|^2} \right. \\ \left. + \alpha \sqrt{|(t_3^x)_{ij}|^2 + |(t_3^y)_{ij}|^2} \right) + \frac{1}{2} \|\mathbf{s} - \mathbf{q}\|^2 \\ + \sum_{i=1}^3 ((\tau_i^x, t_i^x - \mathbf{D}_x s_i) + (\tau_i^y, t_i^y - \mathbf{D}_y s_i)) \\ + \frac{\beta}{2} \sum_{i=1}^3 (\|t_i^x - \mathbf{D}_x s_i\|^2 + \|t_i^y - \mathbf{D}_y s_i\|^2), \end{aligned} \quad (35)$$

where τ_i^x and τ_i^y are Lagrangian multipliers and β is a positive penalty parameter.

According to the classic framework of the ADMM [7], [8], we construct a method to solve (35) with three steps as follows.

Step one: When fixing \mathbf{s} , t_i^x and t_i^y are computed by using the soft shrinkage functions,

$$t_i^{x,y} = \max(0, n_1 - \frac{\lambda_1}{\beta \alpha_1}) \cdot \frac{\mathbf{D}_x s_i - \frac{\tau_i^{x,y}}{\beta}}{n_1}, \quad i = 1, 2, \quad (36a)$$

$$t_3^{x,y} = \max(0, n_2 - \frac{\alpha_1}{\beta \alpha_1}) \cdot \frac{\mathbf{D}_x s_3 - \frac{\tau_3^{x,y}}{\beta}}{n_2}, \quad (36b)$$

where

$$\begin{aligned} n_1 &= \sqrt{\sum_{i=1}^2 (\mathbf{D}_x s_i - \frac{\tau_i^x}{\beta})^2 + (\mathbf{D}_y s_i - \frac{\tau_i^y}{\beta})^2}, \\ n_2 &= \sqrt{(\mathbf{D}_x s_3 - \frac{\tau_3^x}{\beta})^2 + (\mathbf{D}_y s_3 - \frac{\tau_3^y}{\beta})^2}. \end{aligned}$$

Step two: When fixing t_i^x and t_i^y , \mathbf{s} is computed by solving the following minimization problem

$$\begin{aligned} \frac{1}{2} \|\mathbf{s} - \mathbf{q}\|^2 + \sum_{i=1}^3 ((\tau_i^x, t_i^x - \mathbf{D}_x s_i) + (\tau_i^y, t_i^y - \mathbf{D}_y s_i)) \\ + \frac{\beta}{2} \sum_{i=1}^3 (\|t_i^x - \mathbf{D}_x s_i\|^2 + \|t_i^y - \mathbf{D}_y s_i\|^2). \end{aligned}$$

The above minimization problem can be equivalently described by the following real linear system

$$\begin{aligned} (I + \beta \mathbf{D}_x^T \mathbf{D}_x + \beta \mathbf{D}_y^T \mathbf{D}_y) \mathbf{s} \\ = \mathbf{q} + \sum_{i=1}^3 (\mathbf{D}_x^T \tau_i^x + \mathbf{D}_y^T \tau_i^y + \beta \mathbf{D}_x^T t_i^x + \beta \mathbf{D}_y^T t_i^y). \end{aligned} \quad (37)$$

Once \mathbf{s} is computed, we obtain $\mathbf{w} = \mathbf{P}^{-1} \mathbf{s}$.

Step three: The Lagrangian multipliers are updated as follows

$$\tau_i^x = \tau_i^x + \beta(t_i^x - \mathbf{D}_x s_i), \quad \tau_i^y = \tau_i^y + \beta(t_i^y - \mathbf{D}_y s_i), \quad i = 1, 2, 3.$$

• v-subproblem

With \mathbf{u} and \mathbf{w} fixed, the minimization problem (28) is reduced to

$$\arg \min_{\mathbf{v}} \lambda_2 \text{CTV}(\mathbf{v}) + \frac{\alpha_2}{2} \|\mathbf{v} - \mathbf{u}\|^2. \quad (38)$$

This minimization problem can be solved by using a three-step method similar to that of the \mathbf{w} -subproblem. The solution can also be computed by the method given in [2].

To sum up, the (\mathbf{w}, \mathbf{v}) -subproblem need to compute several soft shrinkage functions and solve two real linear systems.

C. New algorithm

Now we present a new algorithm for model (23) based on the methods in Sections IV-A and IV-B. The pseudo code is given in Algorithm 2.

The main idea of Algorithm 2 is to alternately solve (27) and (28) with proper initial values. The only problem left for discussion is how to determine their augmented Lagrange parameters α_i 's. This is one of the well-known parameter-selection problems that stand for a long history. Here, we apply the newly proposed L-surface method in Section III-A to determine the optimal α_i 's. These parameters are determined using a few typical images before running before running Algorithm 2 and, once determined, are used to process all images of the same degradation type.

Now we demonstrate the parameter selection process of α_i 's by the L-surface method in Section III-A. Suppose that we have obtained an observed color image, say 'statues' in

Algorithm 2 Quaternion Operator Splitting Method

```

1: Initialization Choose parameters  $\lambda_1, \lambda_2, \alpha_1, \alpha_2, \tau_i^x, \tau_i^y$  ( $i = 1, 2, 3$ ),  $\alpha, \beta$ . Set the stopping criteria  $tol > 0$  and  $\mathbf{u}^0 = \mathbf{0}, \mathbf{w}^0 = \mathbf{z}, \mathbf{v}^0 = \mathbf{z}, err = 1, err_u = 1, l = 0$ .
2: while  $err > tol$  do
3:    $k = 0, \mathbf{u}^k = \mathbf{u}^l$ 
4:   while  $err_u > tol$  do
5:     Solve  $\mathbf{u}^{k+1}$  by (32) using Algorithm 1,
6:      $k = k + 1$ ,
7:     Compute  $err_u = \frac{\|\mathbf{u}^{k-1} - \mathbf{u}^k\|_2^2}{\|\mathbf{u}^{k-1}\|_2^2}$ ,
8:   end while
9:    $\mathbf{u}^{l+1} = \mathbf{u}^k$ ,
10:  Update  $\mathbf{w}^{l+1}$  by solving (33),
11:  Update  $\mathbf{v}^{l+1}$  by solving (38),
12:   $l = l + 1$ ,
13:  Compute  $err = \frac{\|\mathbf{v}^{l-1} - \mathbf{v}^l\|_2^2}{\|\mathbf{v}^{l-1}\|_2^2}$ .
14: end while

```

Figure 5, under the setting of Example V-A. In case of taking CIEde2000 value as a criterion, we plot the surface of CIEde2000 values according to $\alpha_1, \alpha_2 \in [0, 0.4]$ of restored color images in Figure 3. The optimal parameter is $\alpha_1 = 0.28, \alpha_2 = 0.06$ at which the minimum CIEde2000 value reaches 3.1410.

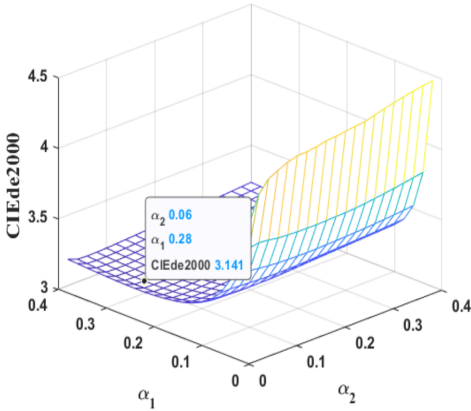


Fig. 3. The values of CIEde2000 for the restored image ‘statues’ in different α_1 and α_2 conditions.

V. NUMERICAL EXPERIMENTS

In this section, we consider various types of cross-channel blur kernels and weight matrices to illustrate the validity of the proposed model and algorithms. We compare the proposed in Algorithm 2 (referred to as Alg. 2) with the CTV₁ [1], CTV₂ [2], the SVTV [21], the split-algorithm-based CTV (for simplicity, the following is referred to as CTV_{split}) [30], MTV [34] by applying them to solve cross-channel deblurring problems. All experiments were performed by MATLAB (R2020a) on a computer with Intel(R) Xeon(R) CPU E5-2630 @ 2.40Ghz/32.00 GB. The stopping criterion for all these

iterative methods is that the norm of the successive iterations is less than 1.0×10^{-5} .

We use the ground truth images shown in Figure 4 to test the image restoration capability of the proposed methods. Let $\mathbf{U}, \hat{\mathbf{U}}$ and \mathbf{U}_m denote the original, observed and restored color images of size $n \times n$, respectively. The quality of the restored color image is indicated by the four standard criteria: PSNR, SSIM, MSE, and CIEde2000. Here, PSNR means the peak signal-to-noise ratio value of \mathbf{U}_m , defined by

$$\text{PSNR}(\mathbf{U}_m, \mathbf{U}) = 10 * \log_{10} \left(\frac{255^2 n^2}{\|\mathbf{U}_m - \mathbf{U}\|_F^2} \right).$$

SSIM denotes the structural similarity index [28] of \mathbf{U}_m and \mathbf{U} , defined by

$$\text{SSIM}(\mathbf{U}_m, \mathbf{U}) = \frac{(4\mu_x\mu_y + c_1)(2\sigma_{xy} + c_2)}{(\mu_x^2 + \mu_y^2 + c_1)(\sigma_x^2 + \sigma_y^2 + c_2)},$$

where x and y respectively stand for the vector forms of \mathbf{U} and $\hat{\mathbf{U}}$, $c_{1,2}$ are two constants, $\mu_{x,y}$ signify the averages of x and y , and $\sigma_{x,y}^2$ stand for the variances of x and y , and σ_{xy} denotes the covariance between x and y . MSE is the mean square error value of \mathbf{U}_m , defined by

$$\text{MSE}(\mathbf{U}_m, \mathbf{U}) = \frac{\|\mathbf{U}_m - \mathbf{U}\|_F^2}{n^2}.$$

The CIEde2000 color difference formula is described in [26], which is used to evaluate the color difference between the original and the restored image.



Fig. 4. Ground truth images

A. Symmetric weight matrix

In this example, we consider the case where all sub-blur kernels are identical and the weight matrix is symmetric. The degraded images used for testing are generated for all models by applying the following cross-channel blur to the clean images,

$$\text{ones}(3, 3) \otimes (G, 5, 5)$$

adding Gaussian noise with standard deviation $\sigma = 0.01$. The weight matrix is chosen as follows

$$W = \begin{bmatrix} 0.7 & 0.15 & 0.15 \\ 0.15 & 0.7 & 0.15 \\ 0.15 & 0.15 & 0.7 \end{bmatrix}.$$

TABLE I
THE VALUES OF PSNR, SSIM, MSE AND CIEDE2000 FOR THE RESTORED IMAGES AT SYMMETRIC WEIGHT MATRIX.

Observed image (PSNR SSIM)	Method	PSNR	SSIM	MSE	CIEde2000	Observed image (PSNR SSIM)	Method	PSNR	SSIM	MSE	CIEde2000
statues (22.6920 0.5002)	CTV ₁	24.7890	0.6817	0.0033	6.3750	waterfall (21.3554 0.5654)	CTV ₁	22.9317	0.7027	0.0051	7.5840
	CTV ₂	24.7416	0.6740	0.0034	6.1065		CTV ₂	22.8933	0.7097	0.0051	7.4116
	CTV _{split}	26.1593	0.6983	0.0024	3.9703		CTV _{split}	25.2652	0.7541	0.0030	3.7826
	MTV	26.9277	0.7374	0.0020	4.0883		MTV	26.3011	0.8008	<u>0.0023</u>	3.7302
	SVTV	27.3174	0.7666	0.0019	<u>3.1070</u>		SVTV	26.6026	0.8132	0.0022	<u>3.1930</u>
	Alg. 2	27.3190	0.7667	0.0019	3.1066		Alg. 2	26.6046	0.8133	0.0022	3.1925
aborigine (21.1179 0.5610)	CTV ₁	22.3146	0.7152	0.0059	7.2164	bear (20.2929 0.5507)	CTV ₁	21.9875	0.7154	0.0063	8.1320
	CTV ₂	22.29382	0.7181	0.0059	7.0597		CTV ₂	21.9315	0.7134	0.0064	8.0203
	CTV _{split}	26.8057	0.7673	0.0021	3.3089		CTV _{split}	23.3130	0.7477	0.0047	4.3142
	MTV	27.7981	0.8107	<u>0.0017</u>	3.3228		MTV	24.3554	0.7907	0.0037	4.3680
	SVTV	28.0820	0.8241	0.0016	<u>2.7849</u>		SVTV	<u>24.5442</u>	0.8063	0.0035	<u>3.7621</u>
	Alg. 2	28.0841	0.8242	0.0016	2.7847		Alg. 2	24.5476	0.8063	0.0035	3.7613
penguin (21.8428 0.6083)	CTV ₁	24.1892	0.7349	0.0038	5.7218	butterfly (20.9821 0.6702)	CTV ₁	22.6934	0.7702	0.0054	7.8815
	CTV ₂	24.1561	0.7389	0.0038	5.3536		CTV ₂	22.6994	0.7789	0.0054	7.7457
	CTV _{split}	25.3151	0.7760	0.0029	4.5552		CTV _{split}	26.8852	0.8355	0.0020	3.0992
	MTV	26.5423	0.8079	<u>0.0022</u>	4.7076		MTV	28.3685	0.8672	<u>0.0015</u>	3.0369
	SVTV	<u>26.5423</u>	0.8166	0.0021	<u>3.5964</u>		SVTV	<u>28.4456</u>	<u>0.8705</u>	0.0014	<u>2.6925</u>
	Alg. 2	26.6801	0.8167	0.0021	3.5954		Alg. 2	28.4609	0.8709	0.0014	2.6896
garden (19.4933 0.5176)	CTV ₁	21.6959	0.7188	0.0068	7.7463	girl (22.5950 0.6946)	CTV ₁	24.0889	0.7844	0.0039	6.9659
	CTV ₂	21.6205	0.7167	0.0069	7.5397		CTV ₂	24.0870	0.7941	0.0039	6.7890
	CTV _{split}	23.7840	0.7741	0.0042	4.9869		CTV _{split}	28.5861	0.8430	0.0014	2.8742
	MTV	25.2706	0.8354	<u>0.0030</u>	4.9658		MTV	29.5834	<u>0.8634</u>	0.0011	2.9632
	SVTV	<u>25.2987</u>	0.8421	<u>0.0030</u>	<u>4.3127</u>		SVTV	<u>29.7722</u>	0.8709	0.0011	<u>2.4627</u>
	Alg. 2	25.3032	0.8423	0.0029	4.3115		Alg. 2	29.7738	0.8709	0.0011	2.4624

We manually tuned the parameters in the three models to make the results solved by each model numerically optimal. In Figures 5 and 6, we give the observed images after the above degradation process, and the restored images of the seven models: The corresponding evaluation criteria for each of the methods used to restore the images are shown in Table I. We observed that the newly proposed methods have the highest PSNR, SSIM, MSE, and CIEde2000 values.

From Figures 5 and 6 we can see that CTV₁ and CTV₂ have a large color shift. The reason for this is that the algorithms corresponding to these methods are designed for within-channel blurring. As a result, only the diagonal blocks of the blur matrix are extracted for processing when considering cross-channel blurring. The CTV_{split} still has some artifacts; see the grass skirt detail in 'aborigine' and the watercress in 'bear'. The MTV has obtained relatively good results visually and numerically when dealing with cross-channel blurring. However, the MTV method seems oversmoothing in some small details; see the flower texture in the upper right corner of the 'butterfly'. Alg. 2 is an algorithms for the SVTV-CTV balance regularization model, which restores images of higher quality under the same stopping criterion. Alg. 2 is more efficient in terms of PSNR, SSIM and CIEde2000 values because it introduces quaternion and thus considers color pixel as a whole.

To further highlight the differences between the MTV and Alg. 2 visual restoration results, we enlarge the local features and display them in Figure 7. The corresponding zoomed portions are denoted with red boxes in Figures 5 and 6. Magnification of local features reveals that Alg. 2 preserves more texture details; see the tip of a tree branch in 'waterfall', the texture of petals in 'butterfly', and the details of the letters in 'garden'. Additionally, we can see color infection at the edges of the MTV restored images, including the part of the hair in 'girl' and the left edge of the flower in 'butterfly' and the lower half of the fence in 'aborigine'.

B. Asymmetric weight matrix

In this example, we consider the restoration results of each method when the sub-blur kernels are different and the weight matrix is asymmetric. For each method, the degraded images are generated by introducing the following cross-channel blur to the clean images,

$$\begin{bmatrix} (A, 5) & (M, 11, 45) & (M, 21, 90) \\ (M, 11, 45), & (A, 5) & (G, 5, 5) \\ (M, 21, 90) & (G, 5, 5) & (A, 5) \end{bmatrix}.$$

adding Gaussian noise with standard deviation $\sigma = 0.01$. The weight matrix is chosen as follows

$$W = \begin{bmatrix} 0.7 & 0.15 & 0.15 \\ 0.1 & 0.8 & 0.1 \\ 0.05 & 0.05 & 0.9 \end{bmatrix}.$$

In Figures 8 and 9, we display the observed images in cross-channel blurring with asymmetric weight matrix, and the restored images of the seven methods. From the visual, CTV₁ and CTV₂ are ineffective at removing cross-channel blur and all show the color shift, for example, the texture of the grass skirt in 'aborigine' is relatively smooth and darker overall. We can observe that in this example the color shift of the images restored by these three methods is smaller than the previous example. This is because a more diagonally dominant weight matrix is used in this example. CTV_{split} shows a significant color shift in this design of asymmetric weight matrix and different sub-blur kernels. The MTV method seems to lose some of the detailed textures and has an oversmoothing effect in the restored images, though it gives relatively good results visually; see the detailed textures on petals of 'butterfly' and rock of 'waterfall'. Later on, we will also zoom in locally to specifically compare the differences between the MTV method and the newly proposed model. As expected, the proposed Alg. 2 achieves better visual results, preserving the geometric textures and color information of the color images.

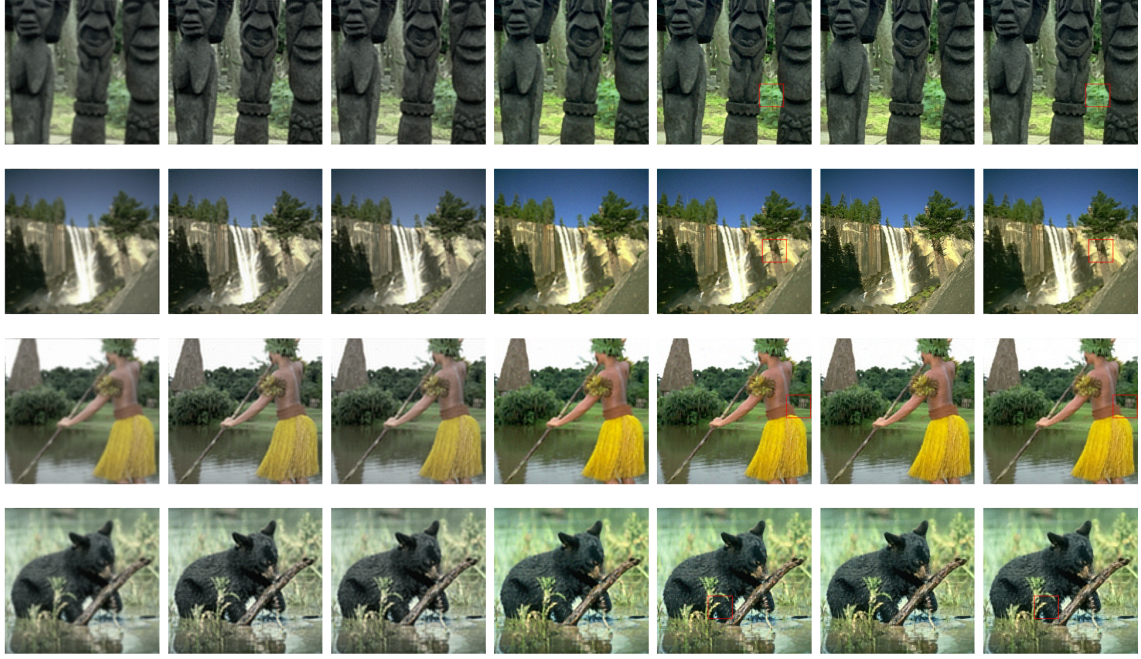


Fig. 5. Restoration results at $\sigma = 0.01$ when the weight matrix is symmetric. (Listed in order are the observed images and the restoration results obtained using CTV₁, CTV₂, CTV_{split}, MTV, SVTV, Alg. 2.)

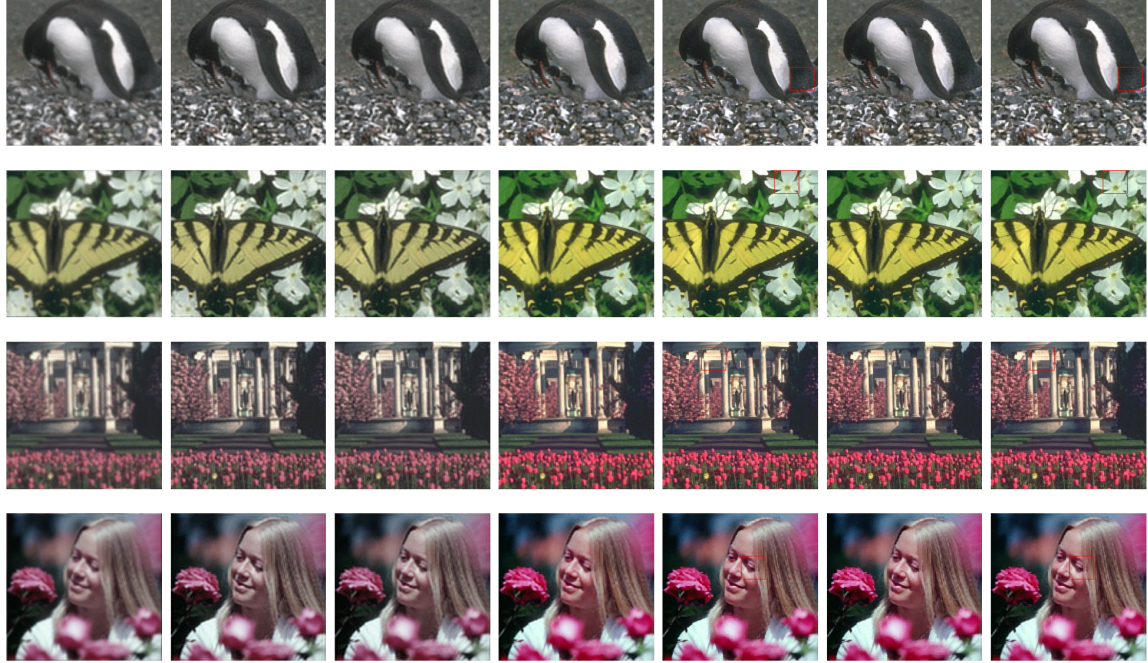


Fig. 6. Restoration results at $\sigma = 0.01$ when the weight matrix is symmetric. (Listed in order are the observed images and the restoration results obtained using CTV₁, CTV₂, CTV_{split}, MTV, SVTV, Alg. 2.)

We then compare the PSNR, SSIM, MSE, and CIEde2000 values of the images restored by these seven methods and show these values in Table II. We evidently observe that the new approach Alg. 2 obtains much higher PSNR, SSIM, MSE, and CIEde2000 values compared to the other methods. Especially for the CIEde2000 criterion, our proposed methods have an average minimum reduction of around 0.64 compared to the

other methods.

To further compare MTV with Alg. 2, we zoom in the local details of the restored images from both methods (the zoomed areas are indicated by red boxes in Figures 8 and 9), as shown in Figure 10. From the comparison of the skin detail in 'aborigine' and the petal textures in 'butterfly', we can see that the newly proposed method produces better results in terms of

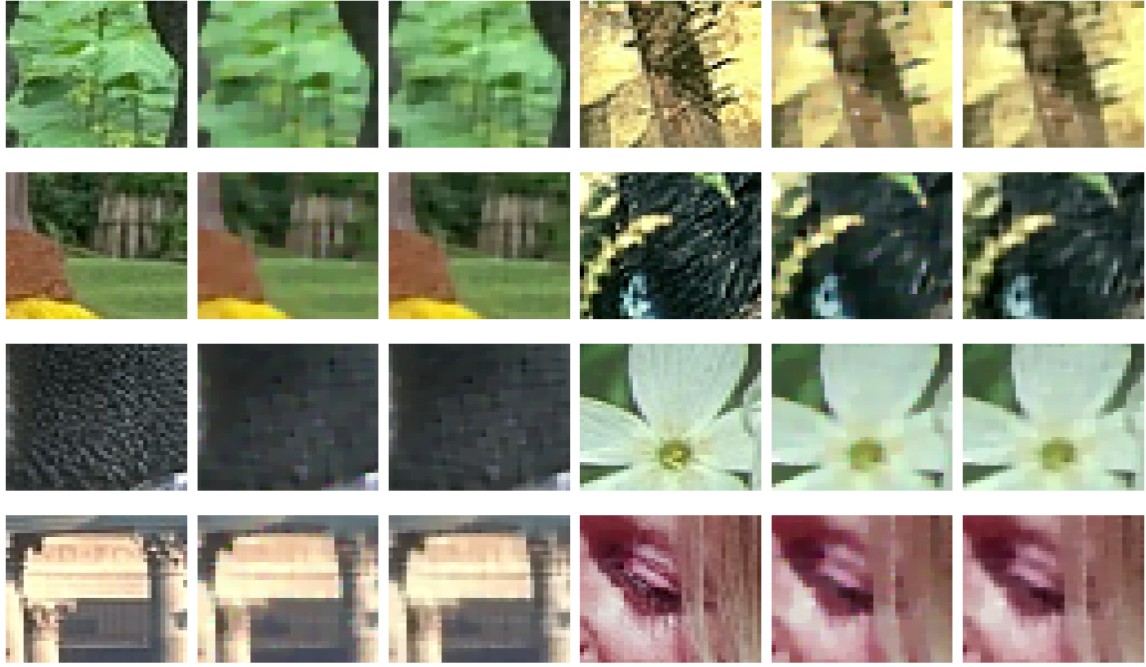


Fig. 7. Corresponding zooming parts is in turn a detail of the original image, restored by the MTV and Alg. 2 models at symmetric weight matrix.

texture features preservation, while the MTV method tends to oversmooth. Also, Alg. 2 produces superior results in terms of color fidelity judging from the branch edges in 'waterfall' and the petal edges in 'butterfly', where the MTV tends to have color infection in the sharply changing areas of the images. Besides, from the comparison between Tables I and II, it is worth emphasizing that the restoration numerical results of the MTV method are worse than the corresponding results in Example V-A in terms of indicators such as CIEde2000, while the two newly proposed methods are more stable for the restoration of different blur kernels. This means that MTV is more sensitive to the design of cross-channel blur kernel, while the newly proposed methods are more general and stable due to the application of the Krylov subspace methods. The above results support the efficiency and superiority of the newly proposed methods.

VI. CONCLUSION

In this paper, we have proposed a novel total variation model for color image cross-channel deblurring using quaternion matrices to represent color images. The proposed model introduces an SVTV-CTV balance regularization term, jointly exploiting the complementary information of the RGB and HSV color spaces. We also present two different iterative algorithms for the proposed model based on the alternating minimization framework. These two iterative algorithms introduce real and quaternion Krylov subspace methods to solve the linear system in the deblurring process, respectively. The numerical results of color image restoration demonstrates the superior performance of the newly proposed method in terms of PSNR, SSIM, MSE and CIEde2000 criteria compared to the existing total variation methods. Furthermore, we demon-

strate the practicality and effectiveness of our newly proposed models and algorithms in addressing medical image artifacts.

ACKNOWLEDGMENT

This work is supported in part by the National Natural Science Foundation of China under grants 12171210, 12090011, and 11771188; the Major Projects of Universities in Jiangsu Province (No. 21KJA110001); the Qing Lan Project of Jiangsu Province; and the Natural Science Foundation of Fujian Province of China grants 2020J05034.

REFERENCES

- [1] T. Blomgren and T. Chan. Color TV: Total variation methods for restoration of vector valued images, *IEEE Trans. Image Process.*, 7: 304–309, 1998.
- [2] X. Bresson and T. Chan. Fast dual minimization of the vectorial total variation norm and applications to color image processing, *Inverse Probl. Imag.*, 2: 255–284, 2008.
- [3] T. Chan, S. Kang, and J. Shen. Total variation denoising and enhancement of color images based on the CB and HSV color models, *J. Visual Commun. Image Repres.*, 12: 422–435, 2001.
- [4] P. Denis, P. Carre, and C. Fernandez-Maloigne. Spatial and spectral quaternionic approaches for colour images, *Comput. Vis. Image Und.*, 107: 74–87, 2007.
- [5] Y. Duan, Q. Zhong, X.-C. Tai, R. Glowinski. A fast operator-splitting method for Beltrami color image denoising, *J. Sci. Comput.*, 92(3): 89, 2022.
- [6] J. Duran, M. Moeller, C. Sbert, and D. Cremers. Collaborative total variation: A general framework for vectorial TV models, *SIAM J. Imaging Sci.*, 9: 116–151, 2016.
- [7] E. Esser. Applications of Lagrangian-Based Alternating Direction Methods and Connections to Split Bregman, *CAM Rep.*, 9, 2009.
- [8] J. Eckstein and D. Bertsekas. On the Douglas-Rachford splitting method and the proximal point algorithm for maximal monotone operators, *Math. Program.*, 55: 293–318, 1992.
- [9] H. Y. Fu, M. K. Ng, and J. L. Barlow. Structured total least squares for color image restoration, *SIAM J. Sci. Comput.*, 28(3): 1100–1119, 2006.

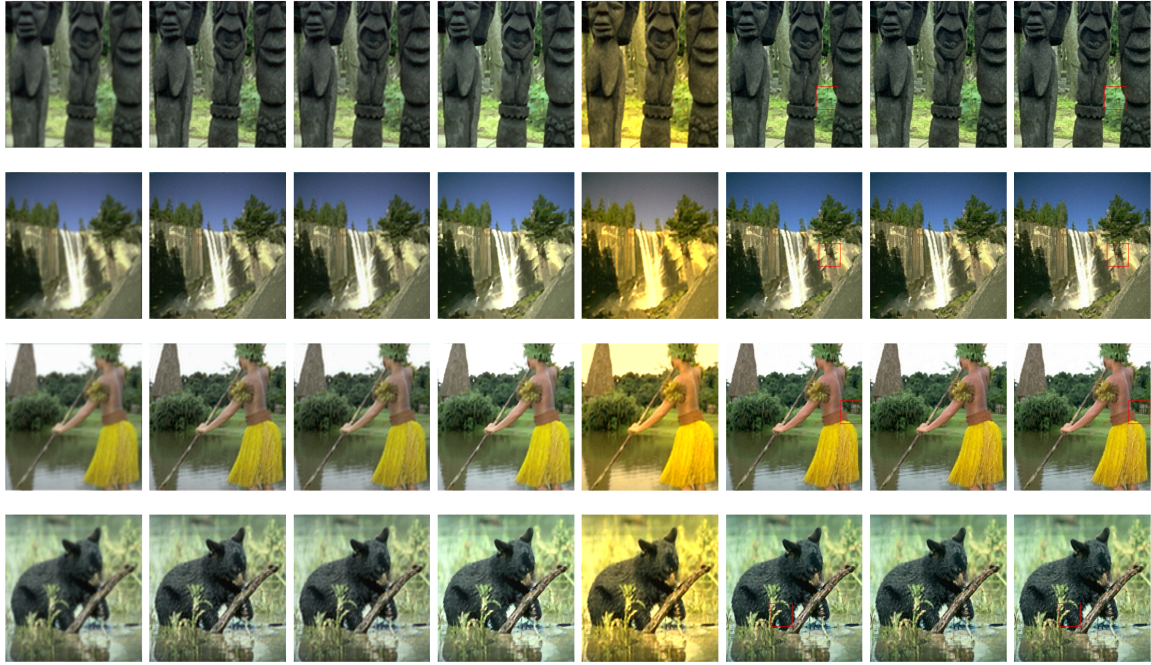


Fig. 8. Restoration results at $\sigma = 0.01$ when the weight matrix is asymmetric. (Listed in order are the observed images and the restoration results obtained using CTV₁, CTV₂, SVTV, CTV_{split}, MTV, SVTV, Alg. 2.)

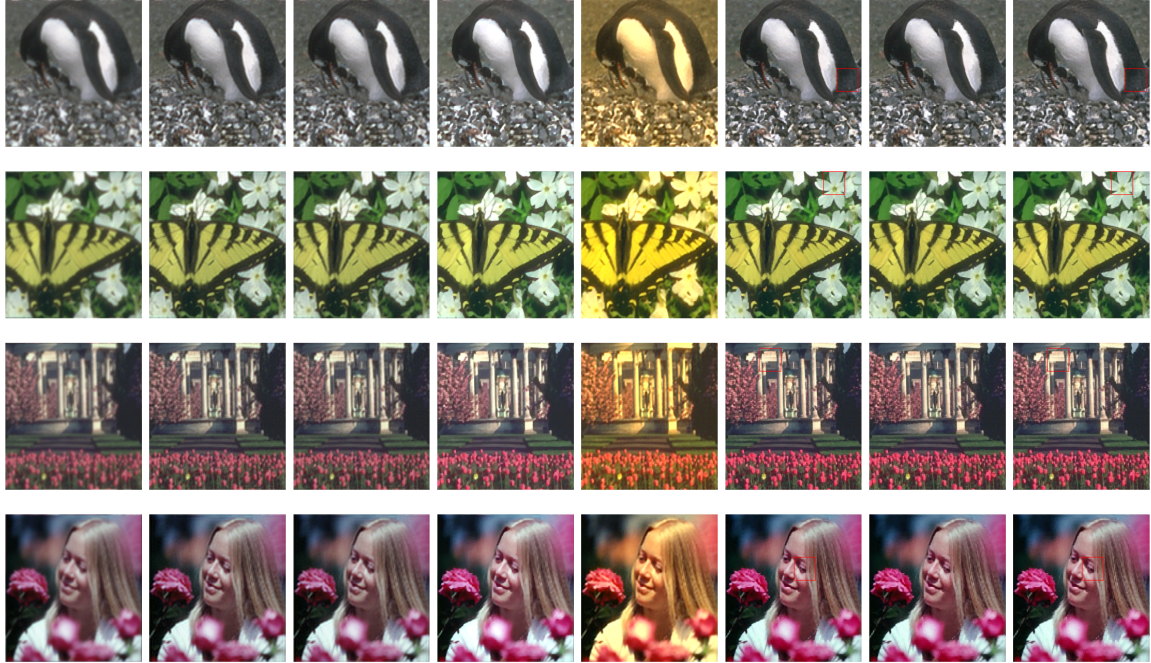


Fig. 9. Restoration results at $\sigma = 0.01$ when the weight matrix is asymmetric. (Listed in order are the observed images and the restoration results obtained using CTV₁, CTV₂, SVTV, CTV_{split}, MTV, SVTV, Alg. 2.)

- [10] H. Y. Fu, M. K. Ng, M. Nikolova, and J. L. Barlow. Efficient minimization methods of mixed l2-11 and 11-11 norms for image restoration, *SIAM J. Sci. Comput.*, 27(6): 1881–1902, 2006.
- [11] N. P. Galatsanos, A. K. Katsaggelos. Methods for choosing the regularization parameter and estimating the noise variance in image restoration and their relation, *IEEE Trans. Image Process.*, 1(3): 322–336, 1992.
- [12] N. P. Galatsanos, A. K. Katsaggelos, R. T. Chin, and A. D. Hillery. Least squares restoration of multichannel images, *IEEE Trans. Signal Process.*, 39: 2222–2236, 1991.
- [13] C. Y. Huang, M. K. Ng, T. T. Wu, and T. Y. Zeng. Quaternion-Based Dictionary Learning and Saturation-Value Total Variation Regularization for Color Image Restoration, *IEEE Trans. Multimedia*, 3769–3781, 2022.
- [14] P. C. Hansen. Analysis of discrete ill-posed problems by means of the L-curve, *SIAM Rev.*, 34(4): 561–580, 1992
- [15] W. R. Hamilton. Elements of Quaternions, *Longmans, Green, and Co*, London, 1866.
- [16] H. Y. Liao, F. Li and M. K. Ng. Selection of regularization parameter

TABLE II
THE VALUES OF PSNR, SSIM, MSE AND CIEDE2000 FOR THE RESTORED IMAGES AT ASYMMETRIC WEIGHT MATRIX.

Observed image (PSNR SSIM)	Method	PSNR	SSIM	MSE	CIEde2000	Observed image (PSNR SSIM)	Method	PSNR	SSIM	MSE	CIEde2000
statues (22.8211 0.4890)	CTV ₁	24.8674	0.6587	0.0033	5.7584	waterfall (21.87546 0.5683)	CTV ₁	23.5651	0.6927	0.0044	6.0229
	CTV ₂	24.8129	0.6510	0.0033	5.4356		CTV ₂	23.5176	0.7005	0.0044	5.8441
	CTV _{split}	18.6735	0.6336	0.0136	14.4771		CTV _{split}	16.2687	0.6819	0.0236	15.3867
	MTV	26.7807	<u>0.7275</u>	<u>0.0021</u>	4.3106		MTV	26.3129	<u>0.7962</u>	<u>0.0023</u>	3.8289
	SVTV	<u>27.3078</u>	0.7641	0.0019	3.1218		SVTV	26.8064	0.8161	0.0021	<u>3.1233</u>
	Alg. 2	27.3089	0.7641	0.0019	3.1214		Alg. 2	26.8077	0.8161	0.0021	3.1229
aborigine (22.3385 0.5643)	CTV ₁	23.8554	0.7054	0.0041	6.0587	bear (20.4969 0.5420)	CTV ₁	22.1822	0.6965	0.0060	6.6658
	CTV ₂	23.8243	0.7091	0.0041	5.8796		CTV ₂	22.1152	0.6947	0.0061	6.5229
	CTV _{split}	15.1137	0.6704	0.0308	15.6282		CTV _{split}	14.9329	0.6858	0.0321	18.1410
	MTV	27.7450	0.8013	<u>0.0017</u>	3.4535		MTV	24.5403	0.7876	<u>0.0035</u>	4.5132
	SVTV	<u>28.2340</u>	<u>0.8230</u>	0.0015	<u>2.6851</u>		SVTV	24.9258	<u>0.8103</u>	0.0032	<u>3.6703</u>
	Alg. 2	28.2353	0.8231	0.0015	2.6849		Alg. 2	24.9279	0.8104	0.0032	3.6697
penguin (21.5152 0.5904)	CTV ₁	23.6758	0.7131	0.0043	6.1883	butterfly (21.5967 0.6596)	CTV ₁	23.6836	0.7609	0.0043	6.1226
	CTV ₂	23.6289	0.7171	0.0043	5.7965		CTV ₂	23.6712	0.7694	0.0043	5.9530
	CTV _{split}	16.1198	0.7181	0.0244	20.1197		CTV _{split}	15.4844	0.7548	0.0283	14.9422
	MTV	26.3597	0.7989	<u>0.0023</u>	4.9455		MTV	28.2452	0.8625	0.0015	3.1680
	SVTV	<u>26.6109</u>	<u>0.8115</u>	0.0022	<u>3.6455</u>		SVTV	28.3127	0.8687	0.0015	<u>2.6089</u>
	Alg. 2	26.6178	0.8117	0.0022	3.6437		Alg. 2	28.3145	0.8688	0.0015	2.6085
garden (19.4949 0.5044)	CTV ₁	21.5268	0.6970	0.0070	7.5611	girl (23.0120 0.6945)	CTV ₁	24.6124	0.7778	0.0035	6.2335
	CTV ₂	21.4425	0.6941	0.0072	7.3168		CTV ₂	24.6185	0.7885	0.0035	6.0251
	CTV _{split}	16.6254	0.6942	0.0217	18.7589		CTV _{split}	16.4629	0.7647	0.0226	18.9103
	MTV	25.0593	0.8270	<u>0.0031</u>	5.2695		MTV	29.3705	<u>0.8552</u>	<u>0.0012</u>	3.1128
	SVTV	<u>25.3852</u>	<u>0.8409</u>	0.0029	<u>4.2331</u>		SVTV	<u>29.7134</u>	0.8666	0.0011	<u>2.4739</u>
	Alg. 2	25.3918	0.8411	0.0029	4.2308		Alg. 2	29.7147	0.8666	0.0011	2.4734

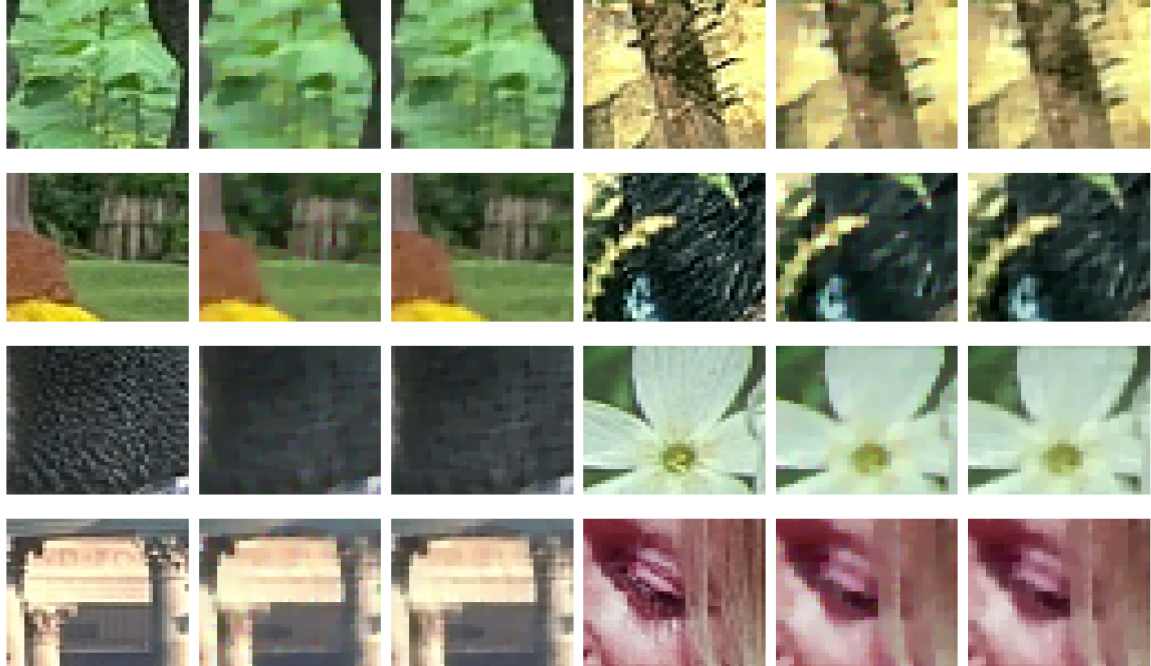


Fig. 10. Corresponding zooming parts is in turn a detail of the original image, restored by the MTV and Alg. 2 models at asymmetric weight matrix.

in total variation image restoration, *JOSA A*, 26(11): 2311–2320, 2011.

[17] H. Liu , X.-C. Tai , R. Kimmel , and R. Glowinski. A color elastica model for vector-valued image regularization, *SIAM J. Imaging Sci.*, 14(2): 717–748, 2021.

[18] H. Liu , X.-C. Tai , R. Kimmel , and R. Glowinski. Elastica models for color image regularization, *SIAM J. Imaging Sci.*, 16(1): 461–500, 2023

[19] Y. Jung. Multiple predicting K-fold cross-validation for model selection, *J. Nonparametr Stat.* 30(1): 197–215, 2018.

[20] Z. G. Jia. The Eigenvalue Problem of Quaternion Matrix: Structure-Preserving Algorithms and Applications, *Science Press*, 2019.

[21] Z. G. Jia, M.K. Ng, and W. Wang. Color Image Restoration by Saturatation-Value (SV) Total Variation, *SIAM J. Imaging Sci.*, 12(2): 972–1000, 2019.

[22] Z. G. Jia and M. K. Ng. Structure-Preserving Quaternion Genenralized Minimal Residual Method, *SIAM J. Matrix Anal. A.*, 42(2): 616–634, 2021.

[23] Z.G. Jia, Q. Y. Jin, M. K. Ng and X. L. Zhao. Non-local robust quaternion matrix completion for large-scale color image and video inpainting, *IEEE Trans. Image Process.*, 31: 3868–3883, 2022.

[24] Z. G. Jia, M. S. Wei, M. X. Zhao, and Y. Chen. A new real structure-preserving quaternion QR algorithm, *J. Comput. Appl. Math.*, 343: 26–48, 2018.

[25] S. Ono and I. Yamada. Decorrelated Vectorial Total Variation, *Proceedings of the IEEE Conference on Computer Vision and Pattern Recognition (CVPR)*, 4090–4097, 2014.

[26] G. Sharma, W. C. Wu, and E. N. Dalal. The CIEDE2000 color-difference formula: Implementation notes, supplementary test data, and mathematical observations, *Color Res. Appl.*, 30: 21–30, 2005.

[27] G. Sapiro. Vector-valued active contours, *Proc. IEEE Conf. Comput. Vis. Pattern Recog. (CVPR)*, 680–685, 1996.

[28] Z. Wang, A. C. Bovik, H.R. Sheikh, and E. P. Simoncelli. Image quality

assessment: from error visibility to structural similarity, *IEEE Trans. Image Process.*, 13(4): 600–612, 2004.

[29] W. Y. Wen and R. H. Chan. Parameter selection for total-variation-based image restoration using discrepancy principle, *IEEE Trans. Image Process.*, 21(4): 1770–1781, 2011.

[30] W. Y. Wen, M. K. Ng, and Y. M. Huang. Efficient Total Variation Minimization Methods for Color Image Restoration, *IEEE Trans. Image Process.*, 17(11): 2081–2088, 2008.

[31] W. Wang, L. Pi, and M. K. Ng. Saturation-Value Total Variation model for chromatic aberration correction, *Inverse Probl. Imag.*, 14: 733–755, 2020.

[32] W. Wang and Q. G. Song. Color image restoration based on saturation-value total variation plus L1 fidelity, *Inverse Probl.*, 38(8): 085009, 2022.

[33] W. Wang, Y. M. Yang, and M. K. Ng. A Spatial Color Compensation Model Using Saturation-Value Total Variation, *SIAM J. Imaging Sci.*, 15(3): 1400–1430, 2022.

[34] J. F. Yang, W. T. Yin, Y. Zhang, Y. L. Wang. A Fast Algorithm for Edge-Preserving Variational Multichannel Image Restoration, *SIAM J. Imaging Sci.*, 2(2): 569–592, 2009.

[35] J. F. Yang, Y. Zhang, and W. T. Yin. An Efficient TVL1 Algorithm for Deblurring Multichannel Images Corrupted by Impulsive Noise, *SIAM J. Imaging Sci.*, 31(4): 2842–2865, 2009.